Memory of pressure-induced superconductivity in a phase-change alloy

Ge Huang,[1,2,3] Zi-Yu Cao,[3] Tian-Ran Wei,[4] Alexander F. Goncharov,[5] Konstantin Glazyrin,[6] Hao Yu,[7,3] Xun Shi,[4] Li-Dong Chen,[4] and Xiao-Jia Chen[3,7,*]

[1]*Key Laboratory of Materials Physics, Institute of Solid State Physics, HFIPS, Chinese Academy of Sciences, Hefei 230031, China*
[2]*University of Science and Technology of China, Hefei 230026, China*
[3]*Center for High Pressure Science and Technology Advanced Research, Shanghai 201203, China*
[4]*State Key Laboratory of High Performance Ceramics and Superfine Microstructure, Shanghai Institute of Ceramics, Chinese Academy of Sciences, Shanghai 200050, China*
[5]*Earth and Planets Laboratory, Carnegie Institution of Washington, D.C., 20015, USA*
[6]*Photon Science, DESY, Notkestrasse 85, DE-22607 Hamburg, Germany*
[7]*School of Science, Harbin Institute of Technology, Shenzhen 518055, China*

(Received 9 February 2021; accepted 12 May 2021; published 24 May 2021)

The application of pressure has been speculated to boost the search for high-temperature superconductors, especially in superhydrides. However, the applied pressure as high as hundreds of GPa needed to create superconductivity in those materials limits their technological application. Finding a route to achieve the high-temperature superconductivity at near-ambient conditions is attractive. By choosing a phase-change alloy $Ge_2Sb_2Te_5$, we study the phase evolution of this material with pressure from the trigonal phase through the amorphous to the body-centered cubic one by the measurements of x-ray diffraction, Raman scattering, resistivity, and Hall coefficient. Superconductivity is observed to take place in the last two phases and can maintain at nearly ambient pressure in the decompression run. Pressure-induced disorder is found to be the key for holding superconductivity in the compressed phase-change alloy.

DOI: 10.1103/PhysRevB.103.174515

I. INTRODUCTION

Two solid states in phase-change materials, amorphous and crystalline, can be produced rapidly and reversibly by heat treatment significantly modifying optical and electronic properties [1–3]. Materials possessing such functional properties enable developments of versatile platforms of a versatile platform for tremendously important applications in memory storage [3–7]. However, for the further improvement of the storage devices a multistate rapid switching material extending binary logic is required [7,8]. Apart from the insulating amorphous phase, by varying degrees of disorder in the crystalline state, one can induce localization of electronic wave functions and hence trigger an insulator-metal transition upon annealing [9]. At the same time, pressure as a fundamental thermodynamic variable can be introduced as a novel stimulus to control disorder in phase-change materials to obtain the multiple resistive states. Considerable efforts have been put forward to study the high-pressure behaviors of the prototypical phase-change material, GeSbTe (GST) compounds along the pseudobinary GeTe × Sb_2Te_3 line [1,10]. At ambient pressure, GST can exist in one amorphous phase and two crystalline phases with metastable rocksalt cubic and stable hexagonal structures, respectively. By applying pressure, the different initial phases of GST experience sequential structural evolutions, which all end up in close-packed bcc structures with similar high density, but varying features depending on the initial composition [11–16]. It has been proposed that disorder in the amorphous and vacancy-rich metastable cubic structure of GST can be additionally modulated leading to a delocalization of the electrons and hence initiating the insulator-metal transitions [11,12]. Therefore, it would be an intriguing task to explore the superconductivity with zero resistivity state in the high-pressure phases of GST.

Exploring superconductivity at high pressures has been of prominent interest for many years. The application of pressure allows to tune the electronic, magnetic, and structural interactions thus affecting the emergence of superconducting states and the superconducting critical temperature (T_c), which can be used to elucidate mechanisms of superconductivity [17–19]. Particularly, superconductors with record-high and even room temperature T_c were synthesized and evidenced by both the zero-resistivity state and Meissner effect at high pressures [20–23]. Nevertheless, the necessity of extreme pressure conditions make these high-T_c superconductors laborious to be employed in the practical applications. How superconductivity achieved by the high pressure approach can be retained upon decompression to low or even ambient pressure remains a great challenge and is on demand. However, the recent example of antimony suggests that the pressure-induced metastable superconducting phases can be retained by following a specific thermodynamic path owing to the associated latent heat of the first-order phase transitions [24]. In the case of $Ge_2Sb_2Te_5$, the difference in the structure of the starting phase leads to a distinct phase sequence on

*xjchen@hpstar.ac.cn

 ©2021 American Physical Society

the compression-decompression cycle even though the high-pressure phase is nominally the same manifesting the phase memory effect [15]. This opens up an opportunity for phase manipulation exploiting the compression-decompression cycle, thus likely making it possible to recover superconducting properties upon the pressure release.

In the pseudobinary GeTe × Sb_2Te_3 system, $Ge_2Sb_2Te_5$ exhibits the best performance in terms of speed and scalability [25]. On the other hand, trigonal $Ge_2Sb_2Te_5$ is shown to be a promising candidate of thermoelectric material [26]. Moreover, the predicted topological nontrivial features in trigonal $Ge_2Sb_2Te_5$ have also drawn great attention [27,28]. The stable trigonal $Ge_2Sb_2Te_5$ holds a nine-layered trigonal structure with cubic close-packed stacking [29]. Nonetheless, the distribution of Ge, Sb, and Te atoms in the specific layers is still a matter of debate. Three different stacking sequences of atomic layers have been proposed to account for the structure of the trigonal phase [29–31]. So far, the initial structure and its evolution with pressure with pressure remain unsettled.

In this work, we report the discovery of superconductivity in $Ge_2Sb_2Te_5$ with structure transformations from the starting trigonal phase in the compression and decompression process. Taking into account the high-pressure behaviors of $GeSb_2Te_4$ [32,33], we further demonstrate the general nature of the emergent superconductivity in high-pressure phases of GST. The trigonal $Ge_2Sb_2Te_5$ characterized as a structure with randomly occupied Ge/Sb layers at ambient goes from the trigonal phase to amorphous and then to the body-centered cubic one with pressure. While pressure is slowly released, most remarkably, we achieve the memory of superconductivity in $Ge_2Sb_2Te_5$ until nearly ambient pressure.

II. EXPERIMENT

$Ge_2Sb_2Te_5$ materials were synthesized by the melting-quenching-annealing method. Raw materials of Ge, Sb, and Te were weighed and sealed in quartz tubes under vacuum in the Ar-filled glove box. The tubes were heated to 1273 K for 10 hours, held at this temperature for 12 hours, and then quenched in water. Afterwards, the tubes were annealed at 853 K for three days. The ingots were ground into fine powders using an agate mortar, and sintered at 773 K at a uniaxial pressure of 50 MPa for 5 minutes by Spark Plasma Sintering (Sumitomo, SPS-2040).

The phase structure of the $Ge_2Sb_2Te_5$ sample at ambient was characterized by using x-ray diffraction (XRD) under Cu Kα radiation ($\lambda = 1.5406$ Å). The high-pressure synchrotron XRD experiments were performed at the PETRA III beamline P02.2 at DESY (Hamburg) with a wavelength of 0.2910 Å. A symmetric diamond anvil cell (DAC) with culet size of 300 μm in diameter was used to generate pressure. Neon was loaded as the pressure transmitting medium to ensure the hydrostatic pressure environment. The pressure was determined by the spectral shift of the ruby fluorescence R1 peak. The DIOPTAS software was used to integrate the raw XRD patterns into two dimensional data set [34]. The data further underwent the Rietveld refinement based on the GSAS package [35].

The temperature-dependent resistivity and thermal conductivity at ambient pressure were measured in a thermal transport option setup by using Quantum Design's Physical Property Measurement System. A miniature nonmagnetic DAC with anvils in a 300-μm culet was employed for the electrical transport and Hall coefficient measurements at high pressures. The cubic boron nitride gasket was preindented to 40 μm in thickness situated between tips of two diamond anvils. Then a 140 μm diameter hole was laser-drilled to act as the sample champer. The $Ge_2Sb_2Te_5$ sample was cut with dimensions of $80 \times 80 \times 15$ μm^3. Four Pt wires were adhered to the sample with the silver epoxy. The electrode leads were electrically insulated from the steel gasket by the *c*-BN (mixed with epoxy) layers. Daphne oil 7373 was used as the pressure transmitting medium. The resistivity and Hall coefficient were obtained using the Van Der Pauw method [36] in Quantum Design's Physical Property Measurement System.

For the high pressure Raman scattering measurements, we used diamond anvils with the ultralow fluorescent background. The preparation of DAC was in the same way as that in the XRD measurements. Raman spectra were collected in back scattering geometry with a laser wavelength of 488 nm by using an in-house system with charge coupled device and spectrometer from Princeton Instrument. The laser power was kept down to 2 mW to avoid damage to the samples.

III. RESULTS AND DISCUSSION

A. Identification of the initial phase

For all proposed stacking sequences of the hexagonal $Ge_2Sb_2Te_5$, the calculated total energy is only slightly different [37]. Owing to the similar electron counts of Sb and Te, distributions of atoms on all positions cannot be analyzed accurately by the powder XRD pattern [38]. However, disorder arising from the mixed Ge/Sb layers would lead to the lower lattice thermal conductivity than that of the ordered layered structures [39]. Figures 1(b) and 1(c) show the temperature dependence of the electrical conductivity σ and thermal conductivity κ of bulk $Ge_2Sb_2Te_5$ from 2 to 300 K. The electronic part κ_{ele} is estimated by the Wiedemann-Franz relation $\kappa_{ele} = L\sigma T$, where L is the Lorenz number ($L = 2.44 \times 10^{-8}$ W Ω K^{-2} in theory for semiconductors). The lattice thermal conductivity κ_{latt} is the difference between κ and κ_{ele}. Hence we can obtain the lattice thermal conductivity of 0.6 $Wm^{-1}K^{-1}$ at 300 K comparable to the value of the Ge/Sb mixed layered structure from the theoretical work. Figure 1(a) shows the XRD pattern of the polycrystalline $Ge_2Sb_2Te_5$. The structure model proposed by Matsunaga *et al.* [29] has been applied to analyze the XRD profile. Combining with the XRD results, the high electrical conductivity and pretty low lattice thermal conductivity obtained from the resistivity and thermal transport measurements, we identify the existence of mixed Ge/Sb layers in the trigonal phase. Thus, the long-standing structure issue [29–31] in this phase-change material has been settled down.

B. Structural evolution with pressure

Figure 2(a) shows the XRD patterns acquired *in situ* of the powdered $Ge_2Sb_2Te_5$ sample at high pressures. The pressure-induced phase transitions can be clearly observed from these patterns and profiles. The initial trigonal phase of $Ge_2Sb_2Te_5$ is confirmed by the diffraction patterns at pressure of 2.3 GPa

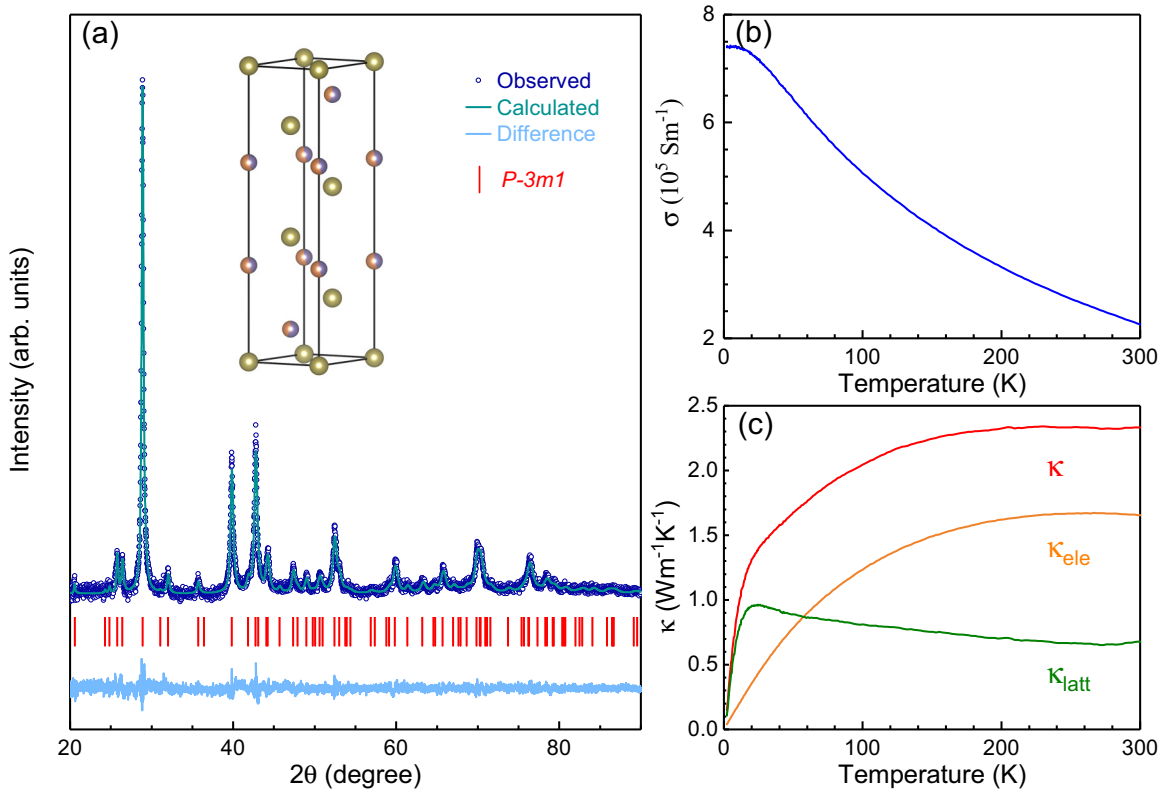

FIG. 1. (a) Measured and calculated XRD profiles of trigonal $Ge_2Sb_2Te_5$ at room temperature, the difference curve is presented at the bottom. The red vertical spikes illustrate the reflection markers. The inset shows its crystal structure. (b) The temperature dependence of electrical conductivity σ from 2 K to 300 K. (c) The temperature dependence of the thermal conductivity κ and its electronic component κ_{ele} and lattice component κ_{latt}.

as shown in the Fig. 2(b). The extracted lattice constants of $a = 4.172$ Å and $c = 16.789$ Å are listed in the lower panel of Fig. 2(b). Upon compression, the intensities of the Bragg peaks decrease and diffuse bands at the different positions appear at pressure above 11.4 GPa, suggesting the amorphization of $Ge_2Sb_2Te_5$. The amorphous phase remains stable until the appearance of a new crystalline phase at pressures above 28.8 GPa. The high-pressure crystalline phase can be regarded as the random solid solution and was indexed as a body centered cubic (bcc) structure with unit cell dimension $a = 3.392$ Å at pressure of 49.8 GPa [Fig. 2(b)] based on the peak positions and their intensities. Figure 2(d) shows the crystalline structures of the trigonal and bcc phases, respectively.

The pressure-dependent lattice parameter(s) and relative unit cell volume are shown in Fig. 2(c). In the pressure range of 11.4 to 28.8 GPa, $Ge_2Sb_2Te_5$ keeps the amorphous phase character. By comparing lattice parameter(s) and lattice symmetry at higher pressures, we could rule out the possibility of the crystalline peaks resulting from the decomposition of $Ge_2Sb_2Te_5$ (Ge, Sb, and Te metals) or the atomic diffusion of steel gasket (Fe) and pressure marker (Au). The volume decrease of the crystalline phases upon compression can be described by the second order Birch-Murnaghan equation of state [40] with the bulk modulus $K_0 = 44 \pm 1$ GPa for the trigonal phase and $K_0 = 85 \pm 4$ GPa for the cubic phase using the first derivative of the bulk modulus $K_0' = 4$ from the previous study [15].

The phase transformation sequences of both $GeSb_2Te_4$ and $Ge_2Sb_2Te_5$ upon compression are summarized as follows: cubic-amorphous-(orthorhombic, for $GeSb_2Te_4$ only)-bcc(c) for the starting meta-stable fcc cubic phase and trigonal-orthorhombic-bcc(h) for the starting stable trigonal phase, respectively [15,16]. By applying pressure, the different initial phases of GST experience sequential structural evolutions, which all end up in close-packed bcc structures with similar high density, but varying features depending on the initial composition. It has been proposed that disorder in the amorphous and vacancy-rich metastable cubic structure of GST can be additionally modulated leading to a delocalization of the electrons and hence initiating the insulator-metal or even insulator-superconductor transitions [11,12,32,33]. However, we found the novel pressure-induced phase transitions routine: trigonal-amorphous-bcc, the difference is likely due to difference in the microstructure of the initial trigonal phase. Therefore, it would be an intriguing task to explore the electronic behavior of $Ge_2Sb_2Te_5$ with pressure.

C. Realization of superconductivity and its reversibility with pressure

Figure 3(a) shows the resistance of $Ge_2Sb_2Te_5$ as a function of temperature in the pressure range of 2.0 to 44.3 GPa. At 13.4 GPa, around the pressure-induced amorphization point, a sharp drop of the resistance below 4 K is clearly observed, suggesting the occurrence of superconductivity within the

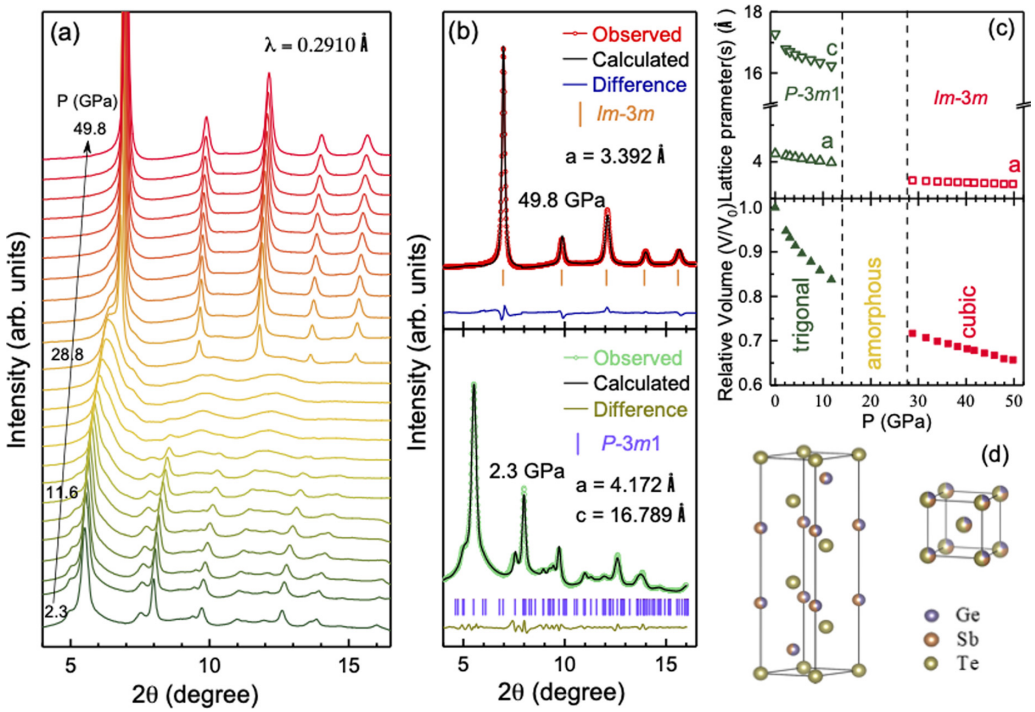

FIG. 2. (a) The XRD patterns at various pressure up to 49.8 GPa. (b) The XRD patterns and Rietveld refinement results at representative pressure of 2.3 GPa and 49.8 GPa. The experimental and fitted data points are plotted together by the open circles and thin curves. The reflection markers are represented by vertical sticks at the lower patterns. The differences between the experiments and calculations are indicated by thin curves at the bottom of each panel. (c) The pressure dependence of the lattice parameter(s) and the normalized unit cell volume per (Te) atom of the trigonal and cubic phases in the pressure range of 0–11.6 GPa and 28.8–49.8 GPa, respectively. (d) The crystalline structures of the *Im*-3*m* and *P*-3*m*1 phases.

amorphous phase. The superconducting transition becomes more obvious with increasing pressure. Upon further compression, T_c suddenly increases to 8.2 K, concomitantly with the entrance of the cubic phase based on the XRD results. Here T_c is defined to be the onset temperature at which the resistance starts to drop. Superconducting state remains up to 44.3 GPa which is highest pressure studied. The zero resistivity state has been achieved in both the amorphous and cubic phases. The suppression of the superconducting state by applied magnetic fields can be observed at pressure of 40.4 GPa [Fig. 3(c)] and 3.9 GPa [Fig. 3(d)]. With increasing magnetic field, T_c decreases gradually. This is characteristic of superconductivity in the high-pressure phases of $Ge_2Sb_2Te_5$.

The typical temperature-dependent resistance curves in the decompression process are plotted in Fig. 3(b). Surprisingly, the sharp superconducting transition in $Ge_2Sb_2Te_5$ persists down to 2.5 GPa with T_c of 4.2 K while releasing pressure. Eventually, the superconductivity cannot be detected at lower pressures and the normal metallic behavior above superconducting state gradually converts into insulating behavior.

Figures 3(c) and 3(d) present the resistance versus temperature at various magnetic fields to trace the upper critical field $\mu_0 H_{c2}$ at selected pressure of 40.4 GPa and 3.9 GPa in the loading and releasing process, respectively. The obtained $\mu_0 H_{c2}$ is 2.9 Tesla at 40.4 GPa and 3.8 Tesla at 3.9 GPa based on the Werthamer-Helfand-Hohenberg (WHH) model. In Figs. 3(c) and 3(d), the colored area represents the temperature dependence of $\mu_0 H_{c2}$ based on the Ginzburg-Landau theory.

The reversible evolution of T_c upon decompression has been reported in In_2Se_3 [41]. Generally, the compound undergoes phase transitions by the applied pressure. In the decompression process, the high-pressure phases hosting superconductivity could be quenched to low pressures until the system returns back to the low-pressure phases. In the case of $Ge_2Sb_2Te_5$, both the rearrangement of atomic structures and the electrical properties are found to be strongly correlated with the evolution of the defects and vacancies. The delay of the phase transition pressure during decompression is due to the frustration of the vacancies since the local order of the intermediate amorphous phase is different from the initial trigonal phase. Thus, the high-pressure superconducting amorphous and cubic phases can persist until pretty low pressures. The retention of superconductivity in $Ge_2Sb_2Te_5$ at nearly ambient pressure provides a hint for practical applications of the near room-temperature superconductivity by introducing disorder in the superhydrides. When the thermal equilibrium is not reached, the vacancies tend to remain disordered after pressure released and the final state is different compared to the initial trigonal phase. The randomly distributed vacancies would trigger the insulator to metal transition [9,42].

D. Examination of phase stability

Raman spectroscopy offers a powerful method for monitoring the evolution of atomic structures during pressure-induced phase transitions through the probe of local vibrational modes.

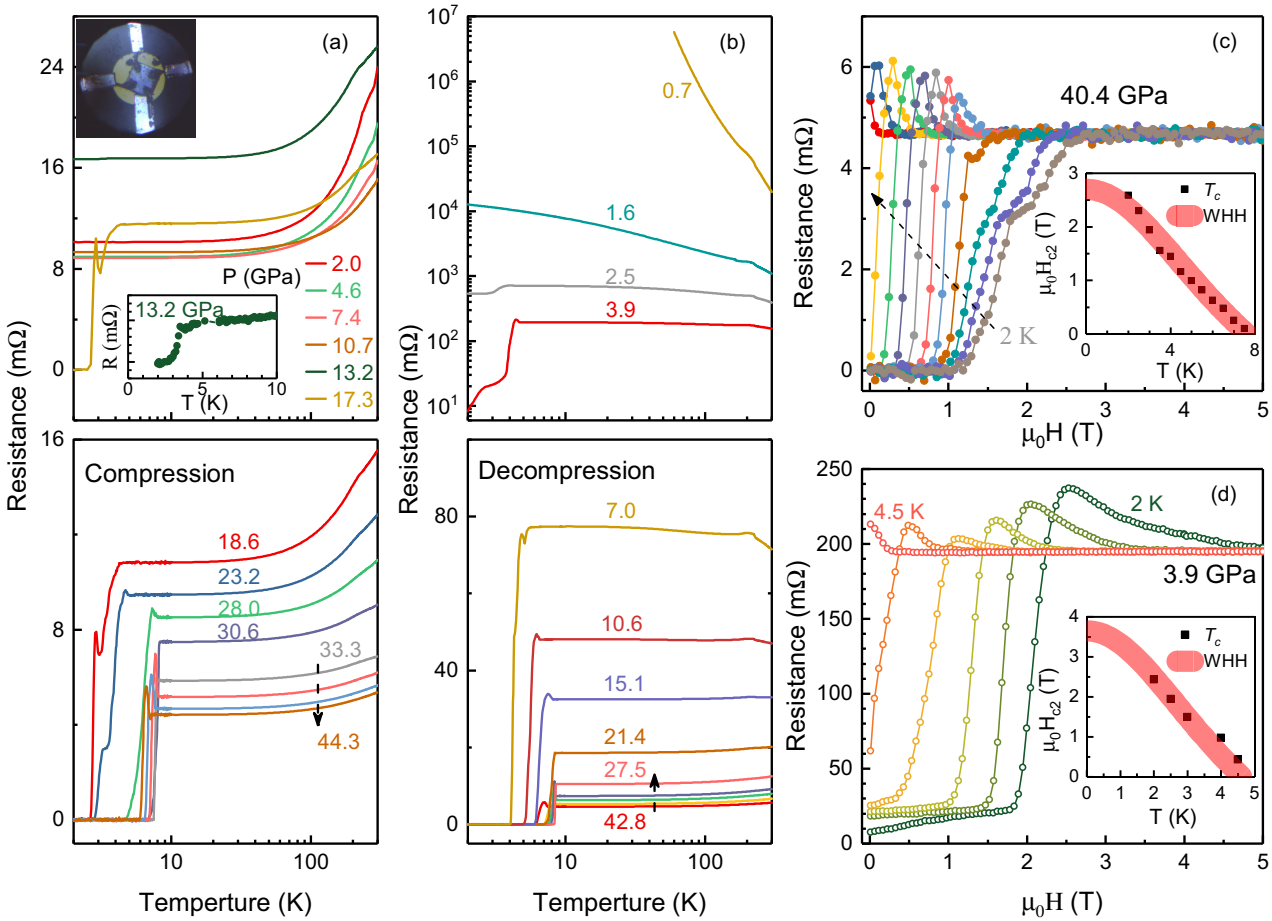

FIG. 3. The representative temperature-dependent resistance of $Ge_2Sb_2Te_5$ in the (a) compression and (b) decompression runs. The upper inset of (a) shows the micrography of $Ge_2Sb_2Te_5$ for the *in situ* electrical transport measurements under pressure. The lower inset of (a) shows the resistance in the temperature range of 2–10 K at the pressure of 13.2 GPa. The magnetic field dependence of the resistance of the $Ge_2Sb_2Te_5$ at various temperatures at the pressure of (c) 40.4 GPa and (d) 3.9 GPa. The solid circles represent the compression data and the open circles represent the decompression data. Inset: The upper critical field μ_0H_{c2} versus temperature. The $\mu_0H_{c2}(T)$ curve is plotted by the color area by using the expression: $\mu_0H_{c2}(T) = \mu_0H_{c2}(0)[1-(T/T_c)^2]/[1+(T/T_c)^2]$ based on Ginzburg-Landau theory.

The trigonal $Ge_2Sb_2Te_5$ belongs to the P-3m1 space group. Therefore, phonon modes at the Γ point can be denoted as $\Gamma = 4(A_{1g} + E_g + E_u + A_{2u})$ according to the irreducible representations. Since the Ge and Sb randomly occupy the same layer, a partial breaking of the P-3m1 symmetry occurs and leads to a lower symmetry state with the P-3m symmetry [43]. Hence the Raman modes of the trigonal phase can be simplified as A-type and E-type with atomic displacements along and perpendicular to the c axis, respectively.

Figure 4(a) shows the Raman spectra of $Ge_2Sb_2Te_5$ for the selected pressures of interest at room temperature. For the Raman spectra obtained at ambient, the peak at 47 cm^{-1}, owing to the A-type Raman mode, can be assigned as the characteristic one of the trigonal phase compared with Raman modes of the metastable cubic phase [44]. In accordance with previous theoretical works, peaks at 94 cm^{-1}, 121 cm^{-1}, and 141 cm^{-1} belong to the E-type Raman-active phonons and peaks at 71 cm^{-1} and 174 cm^{-1} can be attributed to the A-type Raman-active phonons [43]. With increasing pressure, most of the Raman peaks shift toward higher frequencies as shown in Fig. 4(c). The E-type Raman mode (vibrations in the ab plane) at 141 cm^{-1} at ambient pressure presents an anomalous softening tendency with pressure, indicating the instability of the layered structure of the trigonal phase. At 6.6 GPa a new peak appears at 39 cm^{-1} while the peaks of the trigonal phase become weaker and merge. No obvious structural transitions can be deduced on the basis of the XRD measurements (Fig. 2, caption). It implies a possibility of the transformation from the mixed Ge/Sb layered structure [29] to the distinguished layered structure without mixing occupancy [30,31]. Therefore, the strong Raman peak at 39 cm^{-1} can be characterized as an A_{1g} mode which serves as the unique feature of the Kooi structure [43]. The A_{1g} mode softens and persists until the system enters into the cubic phase.

Above 11.6 GPa, the distinct Raman modes at high frequencies gradually become a broad band, suggesting the amorphization of $Ge_2Sb_2Te_5$. The anomalous slope changing of the A-type mode at 200 cm^{-1} can be ascribed to the competition between the hexagonal and amorphous phase. The A_{1g} mode splits into two modes. One of the Raman modes preserves in the cubic phase. For the cubic structure with the Im-3m space group, no Raman-active mode is expected. Our observation on unloading down to 21.3 GPa is consistent with this picture [Fig. 4(b)]. In the loading process, the observed

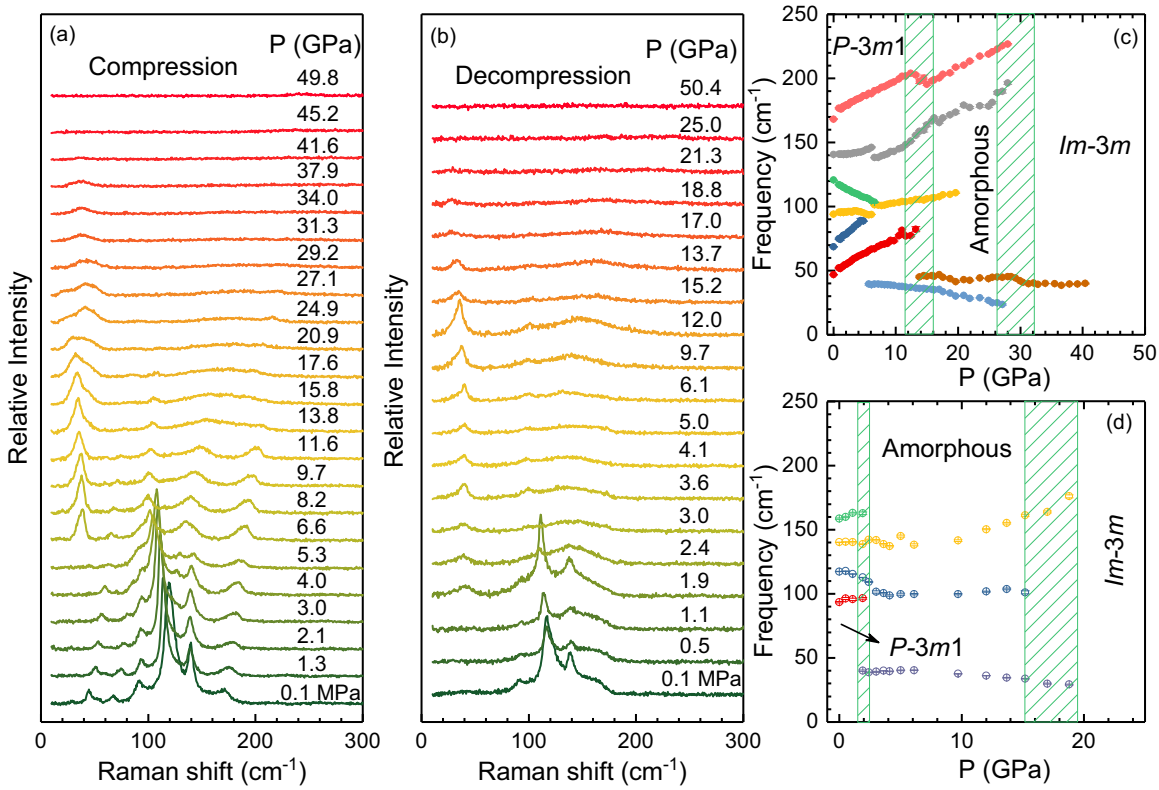

FIG. 4. The typical Raman spectra of $Ge_2Sb_2Te_5$ at room temperature in the (a) compression and (b) decompression runs. The corresponding pressure is marked next to each curve. The pressure dependence of the frequencies of the obtained phonon modes in the (c) compression and (d) decompression runs, respectively. The color shadow area indicates the phase transition region.

Raman peak in the cubic phase could originate from the local symmetry breaking owing to the presence of vacancies and defects upon the crystallization from the amorphous phase. The behaviors of structural evolution obtained by the Raman scattering measurements are similar to the above XRD results.

While pressure is slowly released, the cubic phase first converts into the amorphous phase at 16 GPa as shown in Fig. 4(d). Below 2.4 GPa, most of the Raman peaks can be reproduced as those in the starting hexagonal phase, revealing that the system turns back to the hexagonal structure. However, the absence of the Raman modes at low frequencies suggests the existence of considerable randomly distributed vacancies and defects in the hexagonal structure after a cycle of compression and decompression. Therefore, we can attribute that disorder enhanced by the applying pressure would indeed give rise to a hysteresis in pressure cycling. Consistent with the resistivity measurements, the pressure-induced superconducting cubic and amorphous phases can be preserved until 16 GPa and 2.4 GPa, respectively.

E. Superconducting phase diagram

A comprehensive temperature-pressure phase diagram for $Ge_2Sb_2Te_5$ is mapped out in Fig. 5(a) by combining the XRD, Raman-scattering, and electrical transport measurements. To further understand the close connection between the lattice and electronic structure and physical properties at high pressures, we also measured the Hall coefficient (R_H) for $Ge_2Sb_2Te_5$ at 10 K during the compression and decompression runs. The pressure dependence of the carrier concentration n_H at temperature of 10 K is summarized in Fig. 5(b). The starting trigonal phase presents the *p*-type conduction characteristic with n_H of $\sim 10^{20}$ cm^{-3}, being consistent with the earlier reports [9]. The carrier change from the *p*-type to *n*-type provides another evidence for the phase transition from the trigonal to amorphous structure. Upon further compression, the system still maintains the *n*-type conduction, indicating that the dominant electron carriers are responsible for the superconducting state. During decompression, the electronic properties have similar features as those in the loading process.

For the phonon-mediated superconductivity, T_c mainly depends on the average phonon frequency and electron-phonon coupling constant [45]. The latter can be determined by the combination of the lattice stiffness and electronic stiffness [46]. Owing to the tight connection to the electron density of state at the Fermi surface, the electronic stiffness can be reflected by the obtained value of n_H. The pressure-induced increase in the electronic stiffness usually help to promote T_c [47]. As previously established in the transition metal carbides and nitrides, phonon softening associated with the structural instability leads to the large enhancement of T_c [48,49]. Therefore, the scenario can be applied to account for the evolution of T_c in $Ge_2Sb_2Te_5$ with pressure. The combination of the dramatic increase of n_H with the phonon softening accounts for the occurrence of superconductivity and the later enhancement in the amorphous phase. At higher pressures, the compound enters into a good metal state in a cubic structure

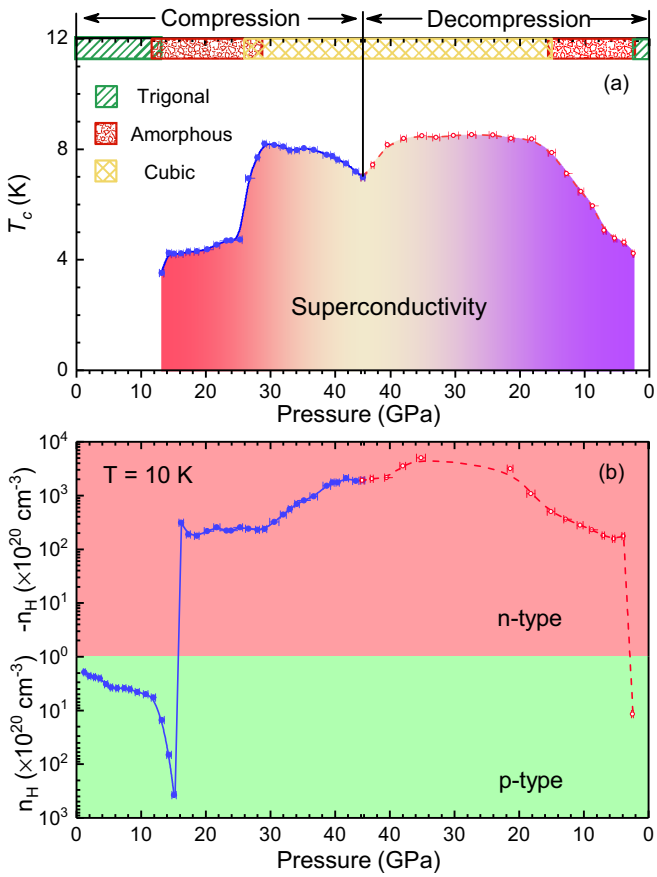

FIG. 5. (a) The phase diagram of $Ge_2Sb_2Te_5$ in the compression and decompression runs. (b) The pressure dependence of the carrier concentration n_H obtained at the temperature of 10 K. The solid circles and the open circles are the data points in the compression and decompression runs, respectively.

but with a higher T_c of $\sim$ 8 K. As the pressure is increased, the difference in the behavior between the increasing n_H and decreasing T_c can be attributed to the phonon stiffening in the cubic phase. When pressure is slowly released, T_c increases and then remains finite due to the decompression-induced phonon softening in the cubic structure. Conversely, phonon modes harden with decreasing pressure and hence lead to the T_c reduction. The T_c vanishes while the system turns back to the trigonal structure.

The interplay between superconductivity and disorder has been discussed for decades. Pressure-induced disorder usually competes with superconductivity in the high-T_c cuprate superconductors [50]. On the other hand, by overcoming the kinetic barrier upon compression, superhydrides possess strong electron-phonon coupling owing to the proximity of electronic and structural instability [51]. Very recently, it is suggested that the metal ions such as lanthanum atoms are "overdoped" with the hydrogen clathrate lattice [52]. Thus, optimizing electron density in the alloy compounds would give rise to extraordinarily high T_c. Through partially substituting the metal ions by adjacent elements, we may expect the order-disorder transitions in superhydrides and hence the near room-temperature superconductors at nearly ambient conditions.

IV. CONCLUSION

In summary, we found the novel high-pressure structural evolution for $Ge_2Sb_2Te_5$ as following pathway: trigonal-amorphous-cubic. Superconductivity emerges in the amorphous and cubic phases during compression and persists until nearly ambient pressure of 2.5 GPa in the decompression process. Disorder triggered by pressure plays a crucial role in the memory effect of the superconductivity for the quenchable high-pressure phases. The disorder in $Ge_2Sb_2Te_5$ is suggested to frustrate the crystallization during decompression. Thus, compressing this typical phase-change material opens an avenue to study the disorder-driven insulator to superconductor transition. During decompression, the metal to insulator transition of $Ge_2Sb_2Te_5$ may be employed in the impending multistate memory devices by introducing chemical pressure or strain. The discovery implies that it is possible to retain the near room-temperature superconductivity at ambient conditions in superhydrides by introducing disorder.

ACKNOWLEDGMENTS

This work was funded through the National Key R&D Program of China (Grant No. 2018YFA0305900) at HPSTAR and the Basic Research Program of Shenzhen (Grant No. JCYJ20200109112810241) at HIT.

[1] N. Yamada, E. Ohno, K. Nishiuchi, N. Akahira, and M. Takao, Rapid-phase transitions of GeTe-Sb_2Te_3 pseudobinary amorphous thin films for an optical disk memory, J. Appl. Phys. **69**, 2849 (1991).

[2] I. Friedrich, V. Weidenhof, W. Njoroge, P. Franz, and M. Wuttig, Structural transformations of $Ge_2Sb_2Te_5$ films studied by electrical resistance measurements, J. Appl. Phys. **87**, 4130 (2000).

[3] M. Wuttig and N. Yamada, Phase-change materials for rewriteable data storage, Nat. Mater. **6**, 824 (2007).

[4] P. Hosseini, C. D. Wright, and H. Bhaskaran, An optoelectronic framework enabled by low-dimensional phase-change films, Nature (London) **511**, 206 (2014).

[5] C. Ríos, M. Stegmaier, P. Hosseini, D. Wang, T. Scherer, C. D. Wright, H. Bhaskaran, and W. H. Pernice, Integrated all-photonic non-volatile multi-level memory, Nat. Photonics **9**, 725 (2015).

[6] T. Tuma, A. Pantazi, M. Le Gallo, A. Sebastian, and E. Eleftheriou, Stochastic phase-change neurons, Nat. Nanotechnol. **11**, 693 (2016).

[7] H. S. P. Wong, S. Raoux, S. Kim, J. Liang, J. P. Reifenberg, B. Rajendran, M. Asheghi, and K. E. Goodson, Phase change memory, Proc. IEEE **98**, 2201 (2010).

[8] D. Lencer, M. Salinga, and M. Wuttig, Design rules for phase-change materials in data storage applications, Adv. Mater. **23**, 2030 (2011).

[9] T. Siegrist, P. Jost, H. Volker, M. Woda, P. Merkelbach, C. Schlockermann, and M. Wuttig, Disorder-induced localization in crystalline phase-change materials, Nat. Mater. **10**, 202 (2011).

[10] N. Yamada and T. Matsunaga, Structure of laser-crystallized $Ge_2Sb_{2+x}Te_5$ sputtered thin films for use in optical memory, J. Appl. Phys. **88**, 7020 (2000).

[11] M. Xu, Y. Meng, Y. Cheng, H. W. Sheng, X. Han, and E. Ma, Pressure-induced crystallization of amorphous $Ge_2Sb_2Te_5$, J. Appl. Phys. **108**, 083519 (2010).

[12] M. Xu, Y. Cheng, L. Wang, H. W. Sheng, Y. Meng, W. Yang, X. Han, and E. Ma, Pressure tunes electrical resistivity by four orders of magnitude in amorphous $Ge_2Sb_2Te_5$ phase-change memory alloy, Proc. Natl. Acad. Sci. USA **109**, E1055 (2012).

[13] A. V. Kolobov, J. Haines, A. Pradel, M. Ribes, P. Fons, J. Tominaga, Y. Katayama, T. Hammouda, and T. Uruga, Pressure-Induced Site-Selective Disordering of $Ge_2Sb_2Te_5$: A New Insight Into Phase-Change Optical Recording, Phys. Rev. Lett. **97**, 035701 (2006).

[14] Y. Q. Cheng, M. Xu, H. W. Sheng, Y. Meng, X. D. Han, and E. Ma, A body-centered-cubic polymorph of the $Ge_2Sb_2Te_5$ phase change alloy, Appl. Phys. Lett. **95**, 131904 (2009).

[15] M. Krbal, A. V. Kolobov, J. Haines, P. Fons, C. Levelut, R. Le Parc, M. Hanfland, J. Tominaga, A. Pradel, and M. Ribes, Initial Structure Memory of Pressure-Induced Changes in the Phase-Change Memory Alloy $Ge_2Sb_2Te_5$, Phys. Rev. Lett. **103**, 115502 (2009).

[16] B. Kalkan, S. Sen, and S. M. Clark, Nature of phase transitions in crystalline and amorphous GeTe-Sb_2Te_3 phase change materials, J. Chem. Phys. **135**, 124510 (2011).

[17] L. Gao, Y. Xue, F. Chen, Q. Xiong, R. Meng, D. Ramirez, C. W. Chu, J. Eggert, and H. K. Mao, Superconductivity up to 164 K in $HgBa_2Ca_{m-1}Cu_mO_{2m+2+\delta}$ (m= 1, 2, and 3) under quasihydrostatic pressures, Phys. Rev. B **50**, 4260 (1994).

[18] X. J. Chen, V. V. Struzhkin, Y. Yu, A. F. Goncharov, C. T. Lin, H. Mao, and R. J. Hemley, Enhancement of superconductivity by pressure-driven competition in electronic order, Nature (London) **466**, 950 (2010).

[19] L. L. Sun, X. J. Chen, J. Guo, P. Gao, Q. Z. Huang, H. Wang, M. Fang, X. Chen, G. Chen, Q. Wu, C. Zhang, D. Gu, X. Dong, L. Wang, K. Yang, A. Li, X. Dai, H. K. Mao, and Z. X. Zhao, Re-emerging superconductivity at 48 kelvin in iron chalcogenides, Nature (London) **483**, 67 (2012).

[20] A. P. Drozdov, M. I. Eremets, I. A. Troyan, V. Ksenofontov, and S. I. Shylin, Conventional superconductivity at 203 kelvin at high pressures in the sulfur hydride system, Nature (London) **525**, 73 (2015).

[21] M. Somayazulu, M. Ahart, A. K. Mishra, Z. M. Geballe, M. Baldini, Y. Meng, V. V. Struzhkin, and R. J. Hemley, Evidence for Superconductivity Above 260 K in Lanthanum Superhydride at Megabar Pressures, Phys. Rev. Lett. **122**, 027001 (2019).

[22] A. P. Drozdov, P. P. Kong, V. S. Minkov, S. P. Besedin, M. A. Kuzovnikov, S. Mozaffari, L. Balicas, F. F. Balakirev, D. E. Graf, V. B. Prakapenka, E. Greenberg, D. A. Knyazev, M. Tkacz, and M. I. Eremets, Superconductivity at 250 K in lanthanum hydride under high pressures, Nature (London) **569**, 528 (2019).

[23] E. Snider, N. Dasenbrock-Gammon, R. McBride, M. Debessai, H. Vindana, K. Vencatasamy, K. V. Lawler, A. Salamat, and R. P. Dias, Room-temperature superconductivity in a carbonaceous sulfur hydride, Nature (London) **586**, 373 (2020).

[24] Z. Wu, L. Z. Deng, M. Gooch, S. Huyan, and C. W. Chu, The retention at ambient of the high-pressure-induced metastable superconducting phases in antimony single crystals, Mater. Today Phys. **15**, 100291 (2020).

[25] D. Lencer, M. Salinga, B. Grabowski, T. Hickel, J. Neugebauer, and M. Wuttig, A map for phase-change materials, Nat. Mater. **7**, 972 (2008).

[26] P. P. Konstantinov, L. E. Shelimova, E. S. Avilov, M. A. Kretova, and V. S. Zemskov, Thermoelectric properties of n(GeTe)-m(Sb_2Te_3) layered compounds, Inorg. Mater. **37**, 662 (2001).

[27] B. Sa, J. Zhou, Z. M. Sun, J. Tominaga, and R. Ahuja, Topological Insulating in GeTe/Sb_2Te_3 Phase-Change Superlattice, Phys. Rev. Lett. **109**, 096802 (2012).

[28] J. Kim, J. Kim, K. S. Kim, and S. H. Jhi, Topological Phase Transition in the Interaction of Surface Dirac Fermions in Heterostructures, Phys. Rev. Lett. **109**, 146601 (2012).

[29] T. Matsunaga, N. Yamada, and Y. Kubota, Structures of stable and metastable $Ge_2Sb_2Te_5$, an intermetallic compound in GeTe-Sb_2Te_3 pseudobinary systems, Acta Crystallogr. Sect. B **60**, 685 (2004).

[30] I. Petrov, R. Imamov, and Z. Pinsker, Electron-diffraction determination of the structures of $Ge_2Sb_2Te_5$ and $GeSb_4Te_7$, Sov. Phys. Crystallogr. **13**, 339 (1968).

[31] B. Kooi and J. T. M. De Hosson, Electron diffraction and high-resolution transmission electron microscopy of the high temperature crystal structures of $Ge_xSb_2Te_{3+x}$ (x= 1, 2, 3) phase change material, J. Appl. Phys. **92**, 3584 (2002).

[32] E. Greenberg, B. Hen, S. Layek, I. Pozin, R. Friedman, V. Shelukhin, Y. Rosenberg, M. Karpovski, M. P. Pasternak, E. Sterer, Y. Dagan, G. K. Rozenberg, and A. Palevski, Superconductivity in multiple phases of compressed $GeSb_2Te_4$, Phys. Rev. B **95**, 064514 (2017).

[33] B. Hen, S. Layek, M. Goldstein, V. Shelukhin, M. Shulman, M. Karpovski, E. Greenberg, E. Sterer, Y. Dagan, G. K. Rozenberg, and A. Palevski, Superconductor-insulator transition in *fcc*$GeSb_2Te_4$ at elevated pressures, Phys. Rev. B **97**, 024513 (2018).

[34] C. Prescher and V. B. Prakapenka, Dioptas: a program for reduction of two-dimensional x-ray diffraction data and data exploration, High Press. Res. **35**, 223 (2015).

[35] B. H. Toby, Expgui, a graphical user interface for gsas, J. Appl. Crystallogr. **34**, 210 (2001).

[36] L. J. van der Pauw, A method of measuring specific resistivity and hall effect of discs of arbitrary shape, Philips Res. Rep. **13**, 1 (1958).

[37] Z. M. Sun, J. Zhou, and R. Ahuja, Structure of Phase Change Materials for Data Storage, Phys. Rev. Lett. **96**, 055507 (2006).

[38] P. Urban, M. N. Schneider, L. Erra, S. Welzmiller, F. Fahrnbauer, and O. Oeckler, Temperature dependent resonant x-ray diffraction of single-crystalline $Ge_2Sb_2Te_5$, Cryst. Eng. Comm. **15**, 4823 (2013).

[39] D. Campi, L. Paulatto, G. Fugallo, F. Mauri, and M. Bernasconi, First-principles calculation of lattice thermal conductivity in crystalline phase change materials: GeTe, Sb_2Te_3, and $Ge_2Sb_2Te_5$, Phys. Rev. B **95**, 024311 (2017).

[40] F. Birch, Finite elastic strain of cubic crystals, Phys. Rev. **71**, 809 (1947).

[41] F. Ke, H. N. Dong, Y. b. Chen, J. B. Zhang, C. L. Liu, J. K. Zhang, Y. Gan, Y. H. Han, Z. Q. Chen, C. X. Gao, J. S. Wen, W. G. Yang, X.-J. Chen, V. V. Struzhkin, H.-K. Mao, and B. Chen, Decompression-driven superconductivity enhancement in In_2Se_3, Adv. Mater. **29**, 1701983 (2017).

[42] M. Wuttig, D. Lusebrink, D. Wamwangi, W. Welnic, M. Gilleen, and R. Dronskowski, The role of vacancies and local distortions in the design of new phase-change materials, Nat. Mater. **6**, 122 (2007).

[43] G. C. Sosso, S. Caravati, C. Gatti, S. Assoni, and M. Bernasconi, Vibrational properties of hexagonal $Ge_2Sb_2Te_5$ from first principles, J. Phys.: Condens. Matter **21**, 245401 (2009).

[44] V. Bragaglia, K. Holldack, J. E. Boschker, F. Arciprete, E. Zallo, T. Flissikowski, and R. Calarco, Far-infrared and raman spectroscopy investigation of phonon modes in amorphous and crystalline epitaxial GeTe-Sb_2Te_3 alloys, Sci. Rep. **6**, 28560 (2016).

[45] W. L. McMillan, Transition temperature of strong-coupled superconductors, Phys. Rev. **167**, 331 (1968).

[46] X. J. Chen, V. V. Struzhkin, Z. G. Wu, R. E. Cohen, S. Kung, H. K. Mao, R. J. Hemley, and A. N. Christensen, Electronic stiffness of a superconducting niobium nitride single crystal under pressure, Phys. Rev. B **72**, 094514 (2005).

[47] W. E. Pickett, A. J. Freeman, and D. D. Koelling, Self-consistent linearized augmented-plane-wave study of the electronic structure and superconductivity of *fcc* lanthanum under pressure, Phys. Rev. B **22**, 2695 (1980).

[48] A. Gauzzi, S. Takashima, N. Takeshita, C. Terakura, H. Takagi, N. Emery, C. Hérold, P. Lagrange, and G. Loupias, Enhancement of Superconductivity and Evidence of Structural Instability in Intercalated Graphite CaC_6 Under High Pressure, Phys. Rev. Lett. **98**, 067002 (2007).

[49] X. J. Chen, Exploring high-temperature superconductivity in hard matter close to structural instability, Matter Radiat. Extremes **5**, 068102 (2020).

[50] J. B. Zhang, V. V. Struzhkin, W. Yang, H. K. Mao, H. Q. Lin, Y. C. Ma, N. L. Wang, and X. J. Chen, Effects of pressure and distortion on superconductivity in $Tl_2Ba_2CaCu_2O_{8+\delta}$, J. Phys.: Condens. Matter **27**, 445701 (2015).

[51] H. Wang, J. S. Tse, K. Tanaka, T. Iitaka, and Y. M. Ma, Superconductive sodalite-like clathrate calcium hydride at high pressures, Proc. Natl. Acad. Sci. USA **109**, 6463 (2012).

[52] V. V. Struzhkin, B. Li, C. Ji, X. J. Chen, V. Prakapen-ka, E. Greenberg, I. Troyan, A. Gavriliuk, and H. K. Mao, Superconductivity in La and Y hydrides: Remaining questions to experiment and theory, Matter Radiat. Extremes **5**, 028201 (2020).